blood

To the editor:

WIP deficiency severely affects human lymphocyte architecture during migration and synapse assembly

Laurène Pfajfer,[1-4,*] Markus G. Seidel,[5,*] Raïssa Houmadi,[3,4] Javier Rey-Barroso,[3,4] Tatjana Hirschmugl,[1,2] Elisabeth Salzer,[1,2] Inés María Antón,[6,7] Christian Urban,[5] Wolfgang Schwinger,[5] Kaan Boztug,[1,2,8,9,†] and Loïc Dupré[1-4,†]

[1]Ludwig Boltzmann Institute for Rare and Undiagnosed Diseases, Vienna, Austria; [2]CeMM Research Center for Molecular Medicine of the Austrian Academy of Sciences, Vienna, Austria; [3]INSERM, UMR1043, Centre de Physiopathologie de Toulouse Purpan, Toulouse, France; [4]Université Toulouse III Paul-Sabatier, Toulouse, France; [5]Division of Pediatric Hematology-Oncology, Department of Pediatrics and Adolescent Medicine, Research Unit for Pediatric Hematology and Immunology, Medical University of Graz, Graz, Austria; [6]Centro Nacional de Biotecnología, Madrid, Spain; [7]Centro de Investigación Biomédica en Red de Enfermedades Neurodegenerativas, Madrid, Spain; [8]Department of Pediatrics and Adolescent Medicine, Medical University of Vienna, Vienna, Austria; and [9]St. Anna Kinderspital and Children's Cancer Research Institute, Department of Pediatrics, Medical University of Vienna, Vienna, Austria

The high motility of immune cells and their ability to establish cell-to-cell contacts depend on a tight regulation of actin cytoskeleton dynamics. Murine studies have identified the Wiskott-Aldrich syndrome protein (WASP)-interacting protein (WIP) as a key regulator of actin dynamics in immune cells.[1-7] Correspondingly, a previously identified WIP-deficient patient suffered from lymphopenia and harbored defects in T-cell proliferation, chemotaxis, and natural killer–mediated cytotoxicity.[8]

We investigated a 2-year-old patient, who had bronchiolitis and viral pneumonia in his first month of life. At 3 months, he developed pneumonitis requiring mechanical ventilation. Cytomegalovirus (CMV) was detected in all tested body fluids. Intermittent episodes of bloody diarrhea suggestive of inflammatory bowel disease or recurrent intussusception required platelet and red blood cell transfusions. The patient exhibited psychomotor delay without evidence of encephalitis. He had hypergammaglobulinemia and a reduced proportion of memory B cells (supplemental Table 1; supplemental Figure 1, available on the *Blood* Web site). Profound $CD4^+$ T-cell lymphopenia was associated with skewing toward an effector memory phenotype. Relative proportions of blood $TCR\gamma\delta^+$ and $CD8^+$ T cells were increased (supplemental Figure 1), most $CD8^+$ T cells also displaying an exhausted effector memory phenotype. In line with the lack of naïve T cells, thymic development appeared abnormal as supported by thymus involution and low T-cell receptor excision circles and thymic emigrants. T-cell proliferative responses were reduced to borderline normal (supplemental Table 1). As the clinical situation of the patient was deemed too severe for a fully conditioned allogeneic hematopoietic stem cell transplantation (HSCT) as performed recently for WIP-deficient patients,[9] sequential infusions of peripheral lymphocytes and stem cells from the HLA-identical mother were performed at the 10th to 13th month of life (Figure 1A), resulting in sustained T-cell engraftment, CMV elimination from peripheral blood, and severe infection cessation until the last follow-up at 2 years of age. Applying a next-generation sequencing (NGS)-panel covering >250 causative primary immunodeficiency genes,[10,11] we identified a homozygous stop-gain mutation in the *WIPF1* gene (c.C373T, p.R125X; Figure 1B), resulting in loss of WIP and WASP expression (Figure 1C), supporting a role for WIP in stabilizing WASP.[2]

Given the rarity of this disease, we aimed to further explore actin dynamics and ultrastructure in human WIP-deficient leukocytes to provide insight into molecular pathomechanisms. WIP-deficient T cells displayed severely impaired migration toward CCL19 and CXCL12 (Figure 1D). Although the migration defect toward CCL19 might in part result from reduced CCR7 expression (supplemental Figure 2), the defect toward CXCL12 was independent of reduced CXCR4 expression, suggesting an intrinsic defect. We further investigated whether actin polarization abnormalities may underlie impaired migration of WIP-deficient T cells. On poly-L-lysine, patient T cells appeared abnormally large, harbored aberrant shapes, and reduced roundness (Figure 1E-F). Upon chemokine stimulation, these cells emitted multiple actin-rich structures, but failed to elongate and to assemble distinct leading and trailing edges (Figure 1E-F). The morphological abnormalities of WIP-deficient T cells were further confirmed by examining side-by-side T cells from patient and donor origin in a blood sample recovered post-DLI. Indeed, residual WIP-negative patient T cells displayed aberrant morphology and reduced ability to elongate (Figure 1G-H).

To assess the role of WIP in B-cell chemotaxis and to verify that the migration defects were a direct consequence of WIP deficiency, we established 2 complementary cellular models. First, WIP expression was knocked down in normal Epstein-Barr virus (EBV)–immortalized B cells (WIP-KD), leading to concomitant loss of WASP expression (supplemental Figure 3A). Second, a tagged WIP construct was stably introduced in patient EBV–immortalized B cells, restoring WIP expression (supplemental Figure 3A). When exposed to a CCL19 gradient in dedicated chambers,[12] WIP-KD cells failed to migrate toward CCL19, as depicted on the tracking maps (supplemental Figure 3B). Accordingly, patient cells failed to migrate toward CCL19, whereas restoration of WIP expression rescued directional migration. Further analysis of cell motility parameters in both models revealed WIP as key regulator of both speed and orientation along the chemokine gradient (Figure 1I). We then studied how WIP deficiency might affect the universal coupling between cell speed and cell persistence. This rule states that fast cells are more directional, because speed promotes actin-dependent maintenance of polarity.[13] We first established that this rule applies to normal B cells exposed to a chemokine gradient, as indicated by the positive correlation between speed and forward migration index (Figure 1J). The slope of this correlation was clearly affected in WIP-KD B cells, indicating that increased speed poorly translated into a gain in directionality and suggesting that WIP controls cell polarity. Indeed, following introduction of LifeAct-GFP in WIP-KD B cells,

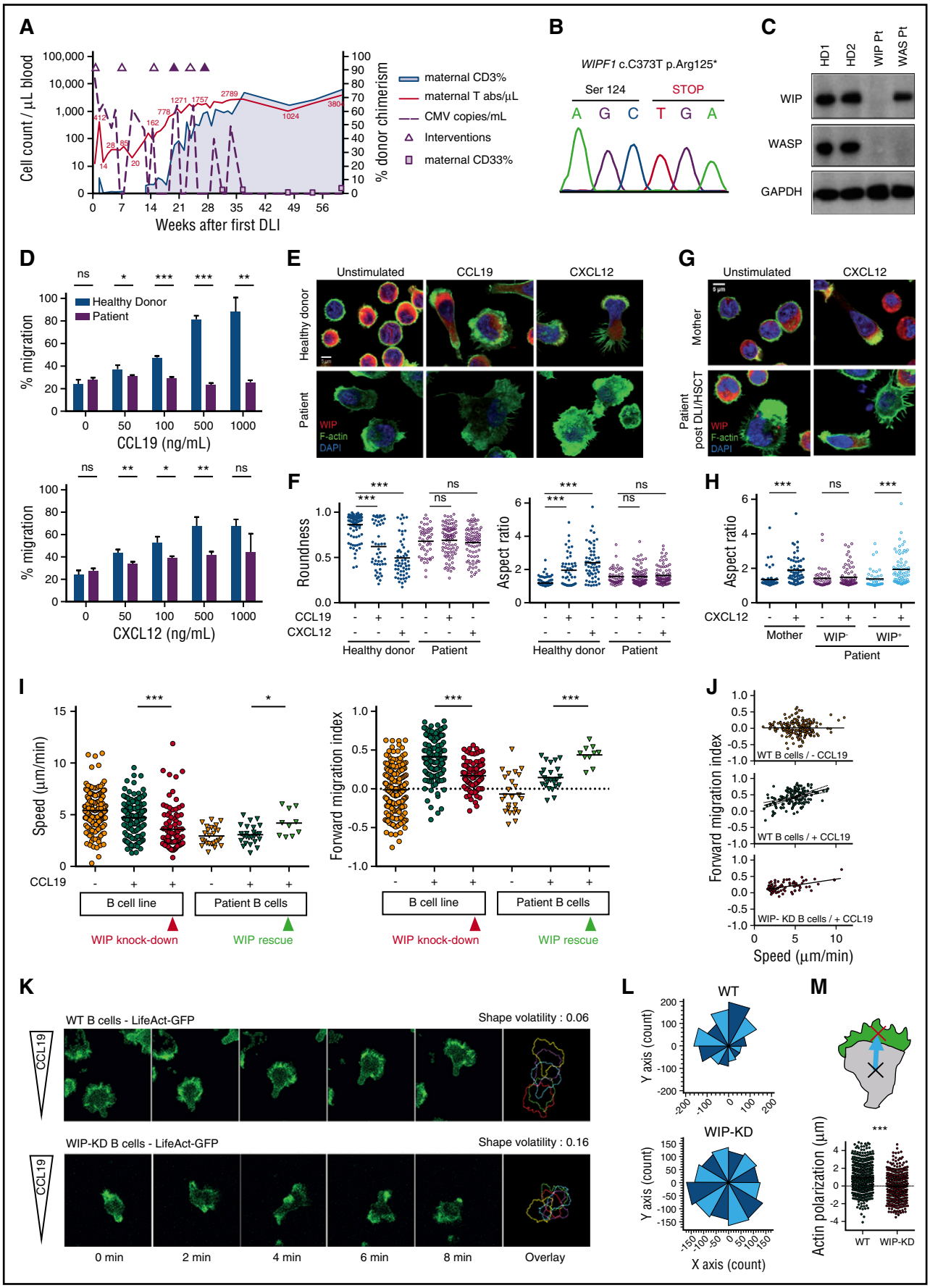

Figure 1.

these cells failed to stabilize a polarized morphology (Figure 1K). The cells emitted large filopodia and pseudopodia in various directions, resulting in abnormally high shape volatility. Consequently, WIP-KD B cells failed to orientate toward CCL19 (Figure 1L) and to polarize actin directionally (Figure 1M). Our study highlights the requirement for WIP in sustaining persistent actin-dependent lymphocyte polarity required for chemokine-evoked directional motility.

Although WIP controls natural killer cell–mediated cytotoxicity via a role in lytic granule polarization,[8,14] its contribution to $CD8^+$ T-cell–mediated cytotoxicity is unknown. Expanded patient $CD8^+$ T cells expressed normal perforin level (Figure 2A), but displayed reduced surface exposure of LAMP1 upon interaction with αCD3-coated P815 cells (Figure 2B). This defective exocytosis translated into reduced target cell killing (Figure 2C). Prolonged interaction with target cells, used to mimic physiological conditions,[15] amplified the killing defect. The reduced capacity of WIP-deficient $CD8^+$ T cells to secrete lytic granules and eliminate target cells may result from a failure to assemble the immunological synapse (IS), a structure that highly depends on actin cytoskeleton dynamics.[16] WIP-deficient $CD8^+$ T cells displayed aberrantly elongated shapes and actin-rich protrusions, both when encountering uncoated and αCD3-coated P815 cells (Figure 2D). In contrast to control cells, WIP-deficient $CD8^+$ T cells failed to assemble an IS and to polarize lytic granules toward target cells (Figure 2E-F). In healthy T cells, WIP and F-actin colocalized at the IS, supporting a role of WIP in actin cytoskeleton remodeling during IS assembly, in addition to its role in lytic granule polarization (Figure 2D). Because the sequential unconditioned DLI/HSCT approach resulted in T-cell chimerism only, we wondered whether the IS between WIP-deficient DCs and normal donor T cells would be affected. Indeed, the DC cytoskeleton has been shown to contribute to T-cell capture[17] and stability of IS.[18] DCs harboring a normal phenotype were differentiated from patient monocytes (data not shown). When coated with superantigens, these cells were able to both capture multiple WIP-positive donor T cells and promote tight contacts (Figure 2G-H), suggesting that the DLI/HSCT procedure normalized IS formation. However, it remains possible that the quality of T-cell activation is impacted by lack of WIP in DCs, calling for cautious follow-up of the patient's ability to mount T-cell responses. To investigate how WIP may control actin cytoskeleton meshwork organization in the context of the IS, we used structured illumination microscopy to image T cells spreading over ICAM-1/αCD3. As expected, control T cells assembled a wide radial structure, the periphery of which was composed of an F-actin ring, consisting of a dense meshwork of short actin fibers (Figure 2I), with WIP forming tiny patches at the IS periphery intermingling with actin filaments. By contrast, WIP-deficient T cells displayed aberrant morphologies, both over ICAM-1/αCD3 (Figure 2I) and poly-L-lysine (supplemental Figure 4A). Zoomed areas of the T cells from the patient revealed aberrant actin organization dominated by elongated filamentous structures. Analysis of actin coherency showed that WIP-deficient T cells were enriched in actin structures oriented in 1 main direction (Figure 2J; supplemental Figure 4B). These data reveal that WIP controls the organization of a reticulated actin meshwork ultrastructure, contributing to the integrity of the cell cortex and sustaining synaptic lamellipodia assembly.

Collectively, we identify WIP as a central protein to control actin meshwork ultrastructure and dynamics required to maintain lymphocyte shape integrity and to assemble lamellipodial protrusions critical for chemotaxis and lytic synapse formation. The severe clinical course of the WIP-deficient patient and the associated lymphocyte defects illustrate the essential role of WIP for human immunity.

*L.P. and M.G.S. contributed equally to this study.

†K.B. and L.D. contributed equally to this study.

The online version of this article contains a data supplement.

Acknowledgments: The authors are grateful to Gareth Jones for the mCherry-WIP encoding lentiviral construct and thank Marion Gröger and Sabine Rauscher from the Core Facility Imaging of the Medical University of Vienna and Andreas Spittler from the Core Facility Flow Cytometry of the Medical University of Vienna. The authors thank Sophie Allart for technical assistance at the Cellular Imaging Facility of TRI-CPTP (Toulouse, France) and Frédérique Gaits-Iacovoni from the Cellular Imaging Facility of TRI-I2MC (Toulouse, France). The authors are grateful to Delphine Guipouy from CPTP (Toulouse, France) and Cecilia Domínguez Conde, Rico Chandra Ardy, and Raúl Jiménez Heredia from LBI-RUD (Vienna, Austria) for technical advice and discussion.

This work was supported in part by the Styrian Children's Cancer Aid Fund (Steirische Kinderkrebshilfe) (M.G.S.) and by the Vienna Science and Technology Fund (WWTF-LS16-060) (K.B. and L.D.), the MINECO/FEDER (SAF2015-70368-R) (I.M.A.), and the French National Agency for Research (ANR-13-BSV1-0031) (L.D.).

Contribution: L.P., M.G.S., K.B., and L.D. designed the study; L.P., M.G.S., R.H., T.H., E.S., and L.D. collected data; L.P., M.G.S., R.H., J.R.-B., T.H., E.S., I.M.A., K.B., and L.D. analyzed and interpreted data; L.P. performed statistical analysis; C.U., W.S., and M.G.S. cared for the patient; L.P., K.B., and L.D. wrote the manuscript with input from M.G.S.; and all authors approved the final version of the manuscript.

Conflict-of-interest disclosure: The authors declare no competing financial interests.

ORCID profiles: L.D., 0000-0002-7278-6503.

Correspondence: Loïc Dupré, INSERM UMR1043, Centre de Physiopathologie de Toulouse Purpan, CHU Purpan, 1, Place du Dr Baylac, 31300 Toulouse, France; e-mail: loic.dupre@inserm.fr; and Kaan Boztug, Ludwig Boltzmann.

Figure 1. Identification of a WIP-deficient patient and of the role of WIP in lymphocyte chemotaxis. (A) Immune reconstitution and plasma CMV load in the patient after sequential infusion of peripheral blood lymphocytes and stem cells from the HLA-identical mother (sequential DLI/HSCT). Doses were calculated for a target number of T cells (from 1×10^6/kg $CD3^+$ to maximum 1×10^7/kg $CD3^+$ cells; white triangles) and stem cells (2×10^7/kg $CD34^+$ plus 2×10^7/kg $CD3^+$ cells; black triangles). Plasma concentration of CMV nucleic acid is shown as copies per milliliter (dotted line, left y-axis). Chimerism of maternal $CD3^+$ T cells is plotted as absolute number (solid line, left y-axis) and proportion (gray-shaded area, right y-axis). (B) Electropherogram of Sanger sequencing depicting the homozygous c.373C>T mutation in *WIPF1*. (C) Western blot analysis of WIP and WASP in EBV–immortalized B cell lysates from 2 healthy donors, the WIP patient and a Wiskott-Aldrich syndrome (WAS) patient. Data were confirmed in 3 independent experiments. (D) Transwell migration of expanded T cells in response to the indicated concentrations of CCL19 and CXCL12. Histograms correspond to the mean ± standard deviation of triplicate values of 1 representative experiment out of 3. (E) Representative pictures of expanded T cells from the patient and a control, following stimulation with CCL19 or CXCL12 and staining for WIP and F-actin. (F) Roundness and aspect ratio values were extracted with ImageJ analysis from 45 to 106 cells per condition. (G) Representative pictures of T cells recovered post-DLI/HSCT, stimulated with CCL19 or CXCL12 and stained for WIP and F-actin. (H) Roundness and aspect ratio values were extracted with ImageJ analysis from 42 to 72 cells per condition. (I) Speed and forward migration index were extracted from the trajectory records of the indicated cells using the Ibidi chemotaxis tool. Data represent 1 representative experiment out of 3. (J) Plots showing correlation between cell speed and forward migration index along the y-axis (chemokine gradient) for the indicated cells. Data represent 1 representative experiment out of 3 performed. (K) Time-lapse video recording of the LifeAct-GFP expressing wt or WIP-KD B cells exposed to a CCL19 gradient, with color plot showing time evolution of cell contour. The volatility values pertain to the representative cells shown in the time-lapse series. (L) Plots representing the cell polarization angle frequency. The CCL19 source is on top. The orientation of the major cell axis was calculated for 400 cell snapshots per condition. (M) Values of actin polarization vector, calculated as the distance between cell and actin centers of mass. The length of the vector was projected along the y-axis to combine actin polarization with cell orientation along the chemokine gradient. Data stem from 400 cell snapshots per condition. DLI, donor lymphocyte infusion; ns, not significant. Pt, patient. $^*P < .05$, $^{**}P < .01$, $^{***}P < .001$.

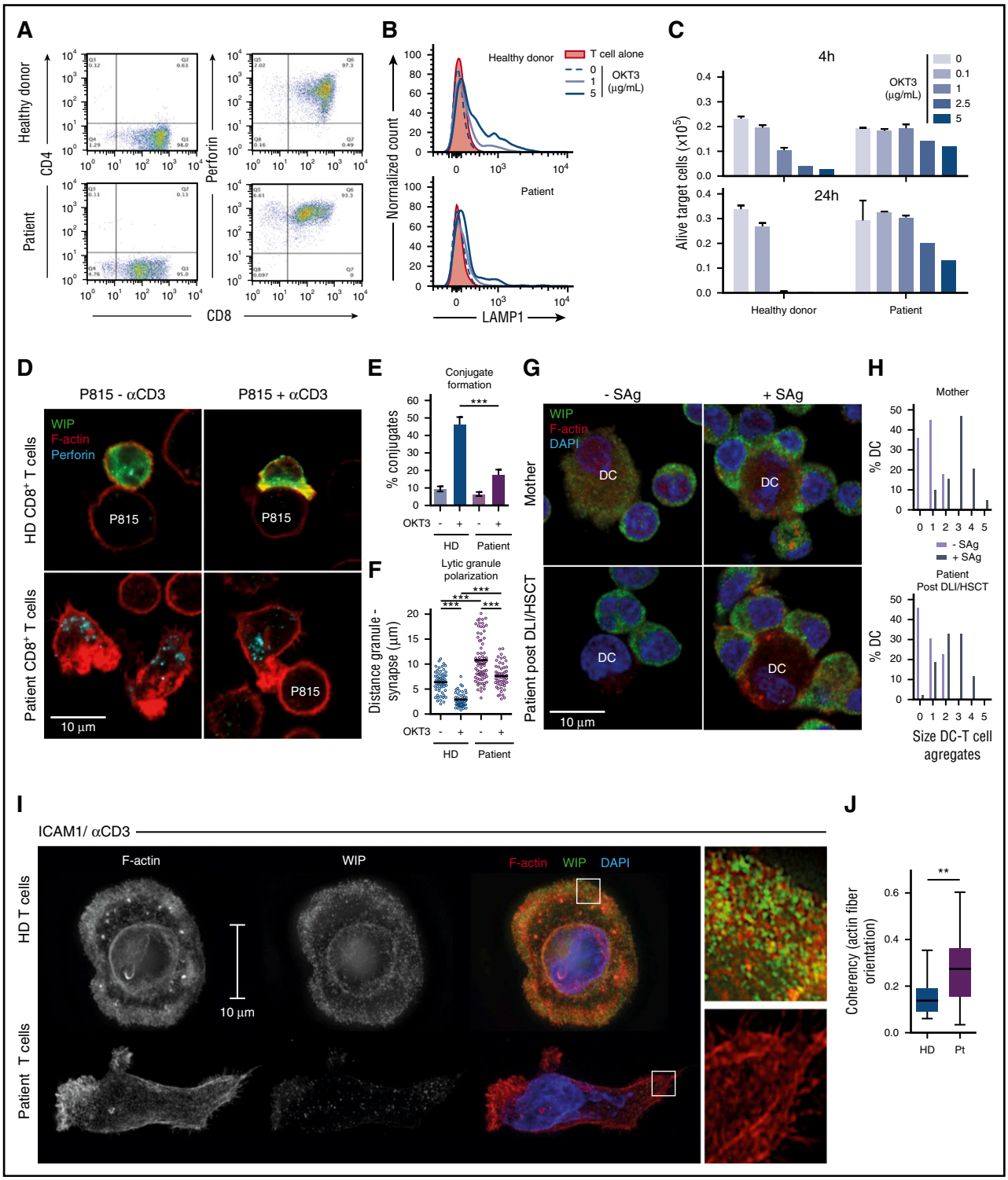

Figure 2. WIP controls CD8$^+$ T lymphocyte cytotoxicity and actin meshwork ultrastructure at the IS. (A) Flow cytometry analysis of CD4, CD8, and perforin expression in purified CD8$^+$ T cells expanded from a healthy donor and the WIP-deficient patient. (B) LAMP-1 expression at the surface of CD8$^+$ T cells upon incubation with P815 cells coated with the indicated concentrations of αCD3 antibody. (C) CD8$^+$ T-cell cytotoxic activity assessed by counting the residual alive P815 target cells after 4 or 24 hours. (D) Representative pictures of healthy donor CD8$^+$ T cells and patient CD8$^+$ T cells forming conjugates with P815 cells coated or not with αCD3 antibody. Fixed conjugates were stained for WIP, F-actin, and perforin. (E) The proportion of T cells forming a synaptic contact with P815 cells was assessed from confocal images. At least 300 cells were analyzed per condition. (F) The distance from lytic granules to the T cell–P815 cell interface was calculated from confocal images. (G) Representative pictures of conjugates formed between T cells and DCs precoated or not with a cocktail of superantigens. Cells were isolated from the blood of the mother or the patient post-DLI/HSCT, as indicated. Fixed conjugates were stained for WIP, F-actin, and 4′,6-diamidino-2-phenylindole (DAPI). (H) The distribution of the number of T cells captured per DC is represented for each indicated condition. (I) Reconstructed structured illumination microscopy images of healthy donor and patient CD8$^+$ T cells spreading over ICAM-1/ αCD3. Staining for WIP, F-actin, and DAPI is shown for a ventral section of 110-nm thickness. Zoomed areas reveal actin meshwork architecture and WIP distribution. (J) The quantification of actin fiber coherency corresponds to the analysis of 20 zoomed areas per condition. DC, dendritic cell. HD, healthy donor. SAg, super-antigens. *$P < .05$, **$P < .01$, ***$P < .001$.

Institute for Rare and Undiagnosed Diseases, Lazarettgasse 14 AKH BT 25.3, A-1090 Vienna, Austria; e-mail: kaan.boztug@rud.lbg.ac.at.

References

1. Antón IM, de la Fuente MA, Sims TN, et al. WIP deficiency reveals a differential role for WIP and the actin cytoskeleton in T and B cell activation. *Immunity*. 2002;16(2):193-204.
2. Chou H-C, Antón IM, Holt MR, et al. WIP regulates the stability and localization of WASP to podosomes in migrating dendritic cells. *Curr Biol*. 2006;16(23): 2337-2344.
3. Gallego MD, de la Fuente MA, Anton IM, Snapper S, Fuhlbrigge R, Geha RS. WIP and WASP play complementary roles in T cell homing and chemotaxis to SDF-1α. *Int Immunol*. 2006;18(2):221-232.
4. de la Fuente MA, Sasahara Y, Calamito M, et al. WIP is a chaperone for Wiskott-Aldrich syndrome protein (WASP). *Proc Natl Acad Sci USA*. 2007; 104(3):926-931.
5. Banon-Rodriguez I, Saez de Guinoa J, Bernardini A, et al. WIP regulates persistence of cell migration and ruffle formation in both mesenchymal and amoeboid modes of motility. *PLoS One*. 2013;8(8):e70364.
6. Massaad MJ, Oyoshi MK, Kane J, et al. Binding of WIP to actin is essential for T cell actin cytoskeleton integrity and tissue homing. *Mol Cell Biol*. 2014;34(23): 4343-4354.
7. Fried S, Matalon O, Noy E, Barda-Saad M. WIP: more than a WASp-interacting protein. *J Leukoc Biol*. 2014;96(5):713-727.
8. Lanzi G, Moratto D, Vairo D, et al. A novel primary human immunodeficiency due to deficiency in the WASP-interacting protein WIP. *J Exp Med*. 2012;209(1): 29-34.
9. Al-Mousa H, Hawwari A, Al-Ghonaium A, et al. Hematopoietic stem cell transplantation corrects WIP deficiency. *J Allergy Clin Immunol*. 2017;139(3): 1039-1040.e4.
10. Erman B, Bilic I, Hirschmugl T, et al. Combined immunodeficiency with CD4 lymphopenia and sclerosing cholangitis caused by a novel loss-of-function mutation affecting IL21R. *Haematologica*. 2015;100(6):e216-e219.
11. Boztug H, Hirschmugl T, Holter W, et al. NF-κB1 haploinsufficiency causing immunodeficiency and EBV-driven lymphoproliferation. *J Clin Immunol*. 2016; 36(6):533-540.
12. Malet-Engra G, Viaud J, Ysebaert L, et al. CIP4 controls CCL19-driven cell steering and chemotaxis in chronic lymphocytic leukemia. *Cancer Res*. 2013; 73(11):3412-3424.
13. Maiuri P, Rupprecht J-F, Wieser S, et al. Actin flows mediate a universal coupling between cell speed and cell persistence. *Cell*. 2015;161(2):374-386.
14. Krzewski K, Chen X, Strominger JL. WIP is essential for lytic granule polarization and NK cell cytotoxicity. *Proc Natl Acad Sci USA*. 2008;105(7): 2568-2573.
15. Vasconcelos Z, Müller S, Guipouy D, et al. Individual human cytotoxic T lymphocytes exhibit intraclonal heterogeneity during sustained killing. *Cell Reports*. 2015;11(9):1474-1485.
16. Dustin ML. Cell adhesion molecules and actin cytoskeleton at immune synapses and kinapses. *Curr Opin Cell Biol*. 2007;19(5):529-533.
17. Benvenuti F, Hugues S, Walmsley M, et al. Requirement of Rac1 and Rac2 expression by mature dendritic cells for T cell priming. *Science*. 2004; 305(5687):1150-1153.
18. Bouma G, Mendoza-Naranjo A, Blundell MP, et al. Cytoskeletal remodeling mediated by WASp in dendritic cells is necessary for normal immune synapse formation and T-cell priming. *Blood*. 2011;118(9):2492-2501.

DOI 10.1182/blood-2017-04-777383

To the editor:

Origins of myelodysplastic syndromes after aplastic anemia

Eiju Negoro,[1,2] Yasunobu Nagata,[1] Michael J. Clemente,[1] Naoko Hosono,[2] Wenyi Shen,[3] Aziz Nazha,[1] Tetsuichi Yoshizato,[4] Cassandra Hirsch,[1] Bartlomiej Przychodzen,[1] Reda Z. Mahfouz,[1] Teodora Kuzmanovic,[1] Mikkael A. Sekeres,[1] Hideki Makishima,[4] Seishi Ogawa,[4] and Jaroslaw P. Maciejewski[1]

[1]Department of Translational Hematology and Oncology Research, Taussig Cancer Institute, Cleveland Clinic, Cleveland, OH; [2]Department of Hematology and Oncology, Faculty of Medical Sciences, University of Fukui, Fukui, Japan; [3]Department of Hematology, The First Affiliated Hospital with Nanjing Medical University, Nanjing, China; and [4]Department of Pathology and Tumor Biology, Graduate School of Medicine, Kyoto University, Kyoto, Japan

The course of aplastic anemia (AA) is often complicated by the development of clonal disorders such as paroxysmal nocturnal hemoglobinuria (PNH) and secondary myelodysplastic syndromes (sMDS).[1-5] Identification of patients at risk for development of sMDS following AA, and distinguishing them from those with primary hypoplastic MDS (hypo-MDS) resembling AA, is important for the timely initiation of appropriate therapy. To determine potential discriminating features, we compared mutational disease evolution patterns among patients with AA, PNH, sMDS, hypo-MDS, and typical primary normo/hypercellular MDS (hyper-MDS).

Bone marrow and/or blood samples were collected from 258 AA and 59 PNH cases at Cleveland Clinic and University Hospital Basel (supplemental Tables 1 and 2, available on the *Blood* Web site). Among them, 35 patients whose initial AA or PNH progressed to sMDS were identified (Table 1; supplemental Tables 1, 2B, and 3). For comparison, we assembled a cohort of 853 patients with primary MDS (pMDS) that included 28 hypo-MDS and 825 hyper-MDS (supplemental Tables 1 and 2A; for details, see supplemental Materials and methods).[6,7] We assessed copy number alterations by single nucleotide polymorphism (SNP) array karyotyping[8,9] and somatic mutations by whole exome sequencing (supplemental Figure 1) and targeted deep sequencing (supplemental Table 4).

First, we analyzed all AA and MDS comparison groups serving as disease controls by targeted deep sequencing (supplemental Table 4). Somatic mutations were detected in 69/133 AA patients (32/71 at presentation vs 42/74 cases after IST; 12 cases were included in both cohorts). In contrast, acquired alterations were detected in 15/23 sMDS patients and in 657/853 pMDS patients (supplemental Figure 2A). As previously shown,[5] most sMDS patients (63%) were characterized by −7/del(7q) evolution (Figure 1A; supplemental Table 3). By comparison, only 14% of pMDS patients had −7/del(7q), as assessed by both metaphase cytogenetics and SNP arrays. The average number of somatic mutations by targeted sequencing was 0.8, 1.0, 1.5, 1.5, and 2.0 in PNH, AA, sMDS, hypo-MDS, and